Supplementary Information

AIE-active organic resonance molecules for highly sensitive dynamic explosive detection

He Jiang, Longyan Zhang, Lijie Xian, Zijie Wang, Jibiao Jin, Chao Zheng*, and Runfeng Chen

State Key Laboratory of Organic Electronics and Information Displays & Institute of Advanced Materials (IAM), Nanjing University of Posts & Telecommunications, 9 Wenyuan Road, Nanjing 210023, China.
Email: iamczheng@njupt.edu.cn.

Table of Contents

1. Materials and synthesis

Materials: All materials and reagents, unless otherwise specified, were purchased from commercial suppliers and used without further purification. Manipulations involving air-sensitive reagents were performed in an atmosphere of dry nitrogen. Tetrahydrofuran (THF), 1,4-dioxane and toluene were dried and purified by routine procedures.

Structure characterization instruments: ^1H and ^{13}C-nuclear magnetic resonance (NMR) spectra were recorded on a Bruker Ultra Shield Plus 400 MHz instrument (400 MHz for ^1H and 100 MHz for ^{13}C, respectively) with dimethyl sulfoxide (DMSO)-d_6 or chloroform-d (CDCl$_3$) as the solvents and tetramethylsilane (TMS, $\delta = 0.00$ ppm) as the internal standards. The quoted chemical shifts are in *ppm* and the coupling constants (*J*) values are expressed in Hz. The splitting patterns have been designed as follows: s (singlet), d (doublet), t (triplet) and m (multiplet). High resolution mass spectra (HRMS) were recorded on a LCT Premier XE (Waters) HRMS spectrometry.
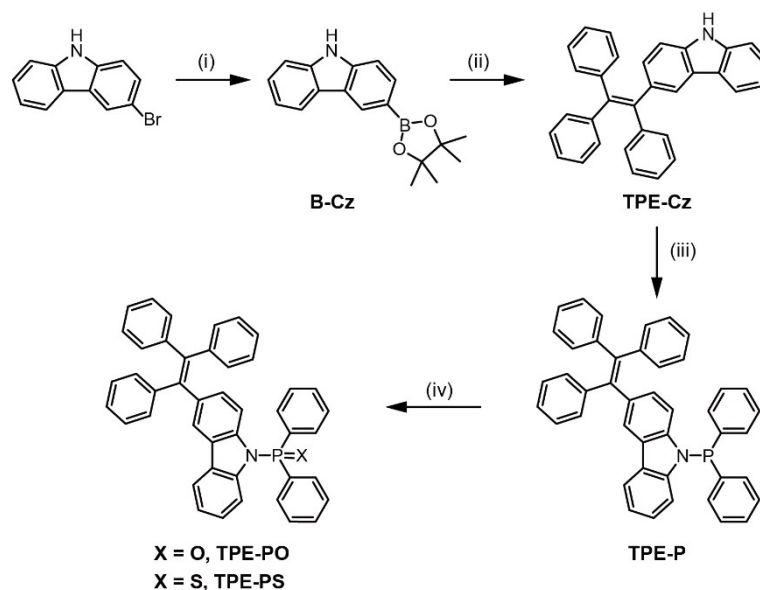
Scheme S1. Synthetic route of AIE-active resonance molecules. (i) bis(pinacolato)diboron, Pd(dppf)Cl$_2$·CH$_2$Cl$_2$, KOAc, 1,4-dioxane, reflux, 24 h; (ii) bromotriphenylethylene, Pd(PPh$_3$)$_4$, K$_2$CO$_3$, toluene, 90ºC, 24 h; (iii) *n*-BuLi, THF, -78ºC, 1 h followed by Ph$_2$Cl, -78ºC, 1 h; (iv) 30% H$_2$O$_2$ (for **TPE-PO**) or sulfur (for **TPE-PS**), CH$_2$Cl$_2$, room temperature, overnight.

Synthesis of 3-(4,4,5,5-tetramethyl-1,3,2-dioxaborolan-2-yl)-9*H*-carbazole (B-Cz)

In an oven dried two-necked flask mixture of 3-bromocarbazole (5.00 g, 20.32 mmol), bis(pinacolato)diboron (6.19 g, 24.38 mmol), 1,1'-bis(diphenylphosphino)ferrocene-palladium(II)dichloride dichloromethane complex (Pd(dppf)Cl$_2$·CH$_2$Cl$_2$) (0.83 g, 1.02 mmol) and potassium Acetate (KOAc) (5.98 g, 60.96 mmol) were taken in dry 1,4-dioxane (50 mL). The reaction mixture was refluxed for 24 h under nitrogen atmosphere. After cooling to the room temperature, the reaction was quenched with water (10 mL) and extracted with dichloromethane (CH$_2$Cl$_2$) (3×30 mL). The organic layers were collected and dried with anhydrous sodium sulphate (Na$_2$SO$_4$). The organic solvent was removed under reduced pressure. The resulting crude product was purified by flash column chromatography on silica gel.[1] Yield: (5.11 g, 86%). ^{1}H NMR (DMSO- d_6, 400 MHz) δ (ppm): 11.43 (s, 1H), 8.46 (s, 1H), 8.21 (d, J = 8 Hz, 2H), 7.71 (d, J = 8 Hz, 1H), 7.48 (t, J = 8 Hz, 2H), 7.40 (t, J = 8 Hz, 1H), 7.18 (t, J = 8 Hz, 1H), 1.33 (s, 12H).
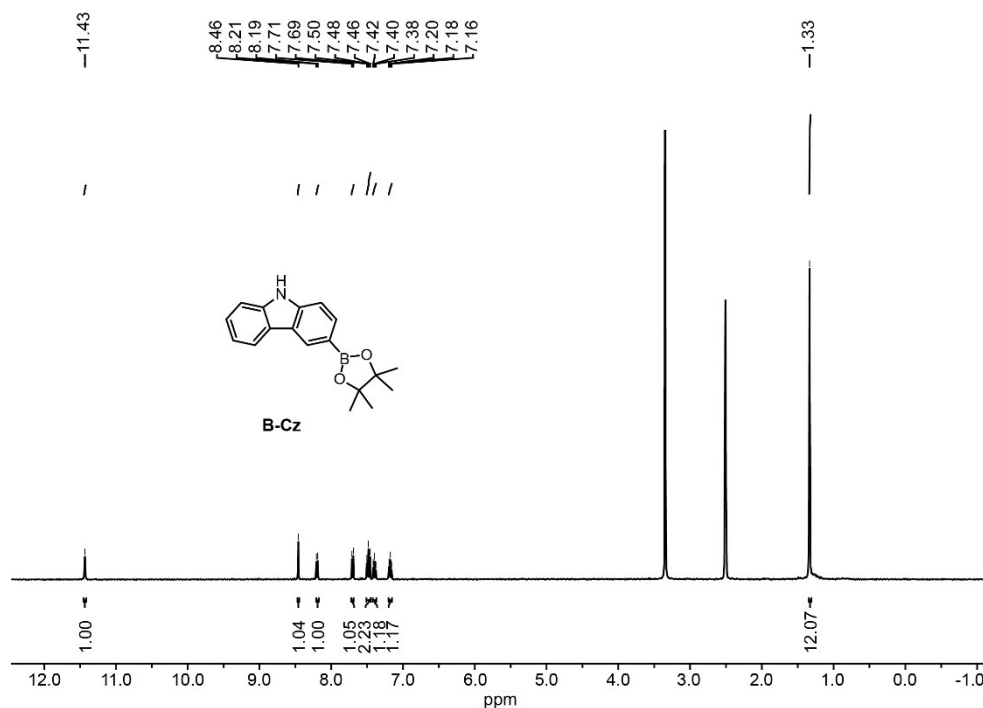

Figure S1. ^{1}H NMR spectrum of **B-Cz** in DMSO- d_6.

Synthesis of 3-(1,2,2-triphenylvinyl)-9*H*-carbazole (TPE-Cz)

To a solution of **B-Cz** (4.00 g, 13.64 mmol), bromotriphenylethylene (4.57 g, 13.64 mmol), tetrakis(triphenylphosphine)palladium Pd(PPh$_3$)$_4$ (0.47 g, 0.41 mmol) and methyltrioctylammonium chloride (0.06 g, 0.14 mmol) in toluene (200 mL), aqueous potassium carbonate (68 mL, 2 M) was added. The reaction mixture was stirred at 90°C for 24 h. After cooling

to room temperature, the reaction was quenched with water (10 mL) and extracted with CH_2Cl_2 (3×30 mL). The organic layers were collected and dried with anhydrous Na_2SO_4 and the organic solvents were removed under reduced pressure. The resulting crude product was purified by flash column chromatography on silica gel.[2] Yield: (5.02 g, 87%). ^{1}H NMR (DMSO- d_6, 400 MHz) δ (ppm): 11.21 (s, 1H), 7.85 (d, J = 8 Hz, 1H), 7.68 (s, 1H), 7.44 (d, J = 8 Hz, 1H), 7.33 (t, J = 8 Hz, 1H), 7.23 (d, J = 8 Hz, 1H), 7.08 (m, 17H).
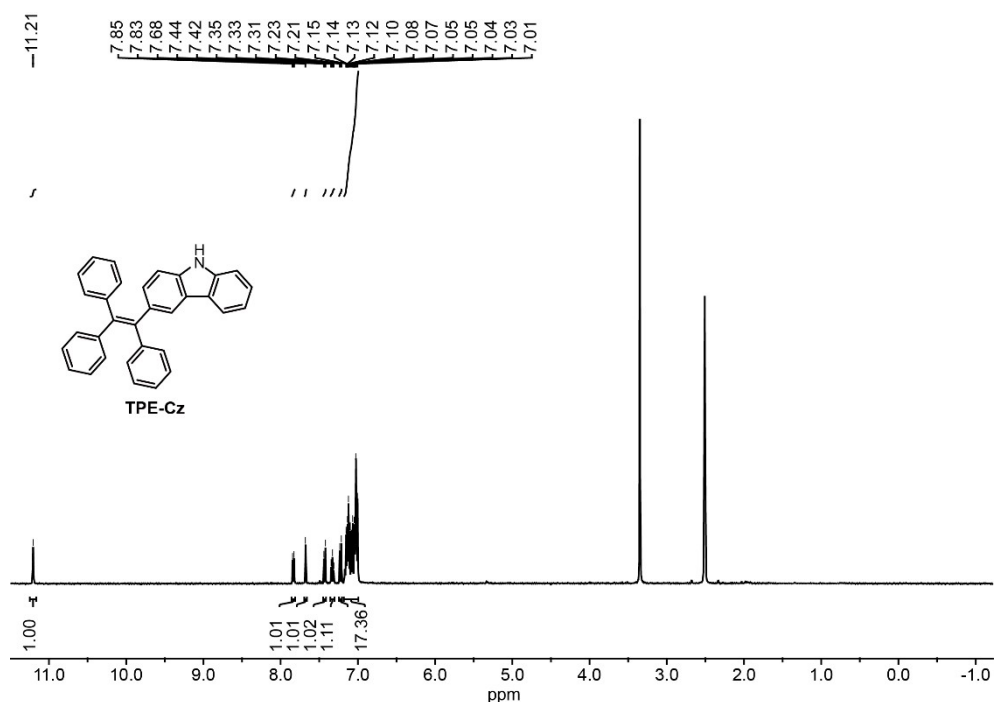

Figure S2. ^{1}H NMR spectrum of **TPE-Cz** in DMSO- d_6.

Synthesis of 9-(diphenylphosphanyl)-3-(1,2,2-triphenylvinyl)-9*H*-carbazole (TPE-P)

To a freshly distilled THF (40 mL) solution of **TPE-Cz** (2.00 g, 4.74 mmol) at -78°C under a nitrogen atmosphere, *n*-butyl lithium (3.6 mL, 5.76 mmol, 1.6 M in hexane) was added dropwise. After lithiation at -78°C for 1 h, dichlorophenylphosphine (Ph_2PCl) (1.05 g, 4.74 mmol) was added into the reaction system rapidly. The reaction mixture at -78°C was allowed to warm to room temperature and stirred overnight. Then, the reaction was quenched with water (10 mL) and extracted with CH_2Cl_2 (3×30 mL). The organic layers were collected and dried with anhydrous Na_2SO_4. The organic solvents were removed under reduced pressure. The resulting crude product was purified by flash column chromatography on silica gel.[3] Yield: (2.15 g, 75%). ^{1}H NMR (DMSO- d_6, 400 MHz) δ (ppm): 7.92 (d, J = 8 Hz, 1H), 7.75 (d, J = 1.6 Hz, 1H), 7.44 (m, 6H), 7.36 (m, 5H), 7.23 (m, 2H), 7.16 (m, 17H). ^{13}C NMR ($CDCl_3$, 100 MHz) δ (ppm): 144.22, 144.15,

144.12, 143.98, 143.91, 142.50, 141.39, 140.49, 136.44, 134.50, 134.36, 131.60, 131.47, 131.44, 131.24, 129.65, 129.23, 128.65, 128.59, 127.62, 126.40, 126.27, 126.21, 126.13, 125.51, 125.42, 122.83, 120.63, 120.05, 113.83, 113.71, 112.87, 112.75. HRMS (EI): m/z calcd for $C_{44}H_{32}NP$ [$M+Na$]$^+$: 628.2170; found: 628.2173.
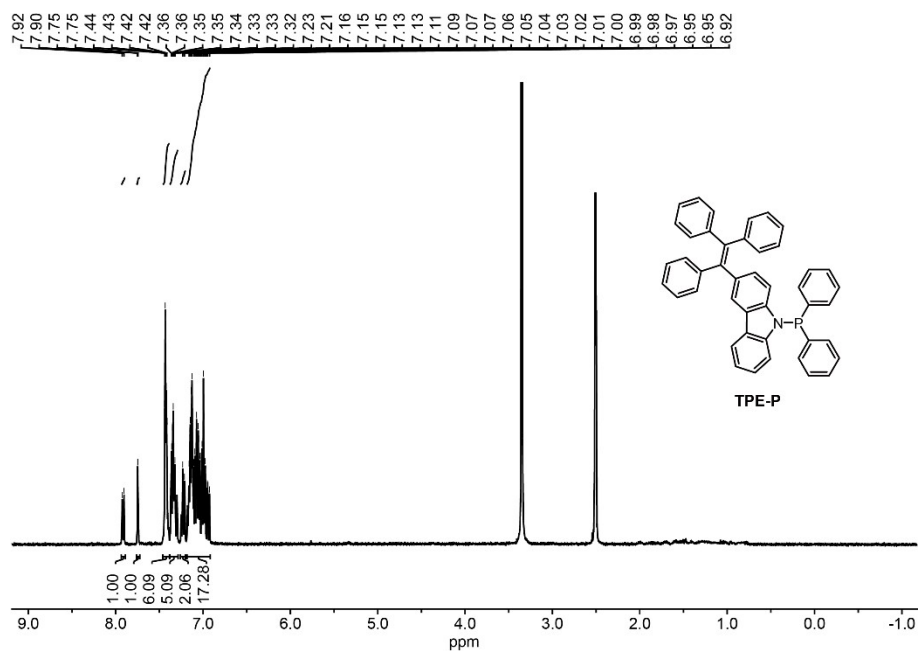

Figure S3. ^{1}H NMR spectrum of **TPE-P** in DMSO- d_6.
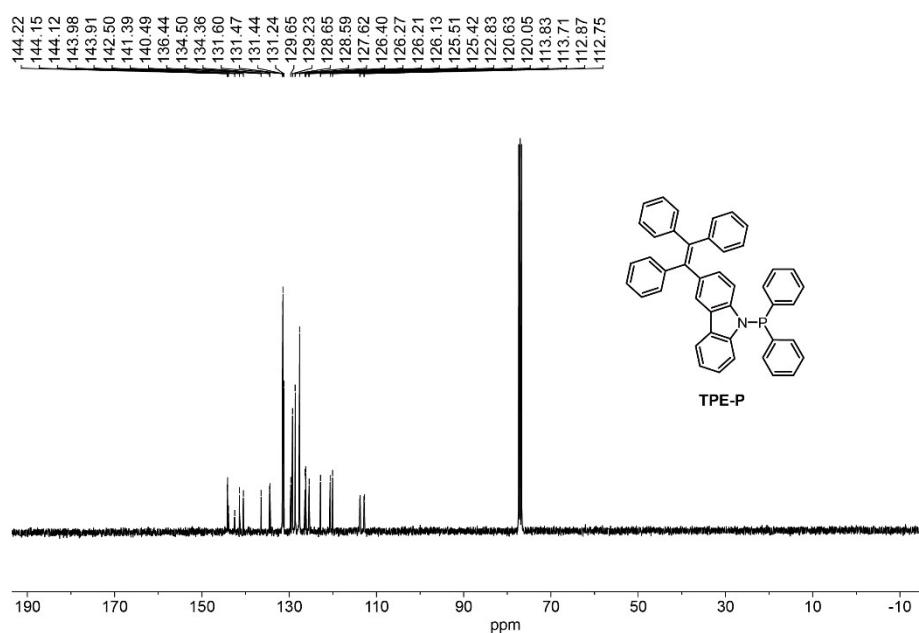

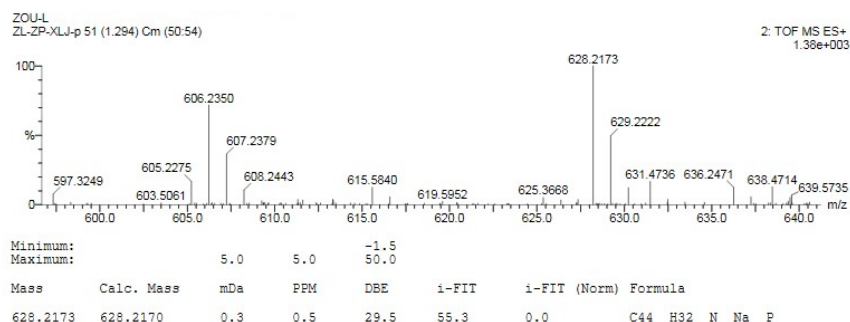**Figure S4.** ^{13}C NMR spectrum of **TPE-P** in CDCl$_3$.

Figure S5. HRMS spectrum of **TPE-P**.

Synthesis of diphenyl(3-(1,2,2-triphenylvinyl)-9*H*-carbazol-9-yl) phosphine oxide (TPE-PO)

TPE-PO was prepared by oxidizing **TPE-P** using hydrogen peroxide (H_2O_2). A 100 mL round-bottom flask was charged with **TPE-P** (2.00 g, 3.30 mmol), CH_2Cl_2 (30 mL), and 30% H_2O_2 (0.4 mL, 12.10 mmol) for the following oxidation. After stirring overnight at room temperature, water (10 mL) was added to quench the reaction. The mixture was extracted with CH_2Cl_2 (3×30 mL) and the collected organic layers were dried with anhydrous Na_2SO_4. The organic solvent was removed under reduced pressure. The resulting crude product was purified by flash column chromatography on silica gel.[4] Yield: (1.85 g, 90%). ^{1}H NMR (DMSO- d_6, 400 MHz) δ (ppm): 7.93 (d, J = 8 Hz, 1H), 7.74 (m, 3H), 7.68 (m, 8H), 7.23 (m, 19H), 6.86 (dd, J = 4 Hz, 1H). ^{13}C NMR ($CDCl_3$, 100 MHz) δ (ppm): 143.88, 143.82, 141.97, 141.94, 140.93, 140.86, 140.31, 140.28, 137.63, 133.13, 133.10, 132.18, 132.07, 131.50, 131.48, 131.38, 130.25, 130.07, 129.08, 128.95, 127.66, 127.64, 126.57, 126.51, 126.45, 126.36, 126.34, 126.16, 126.08, 126.02, 122.63, 121.87, 119.86, 115.06, 114.13 HRMS (EI): m/z calcd for $C_{44}H_{32}NPO$ [$M+Na$]$^+$: 644.2119; found: 644.2113.

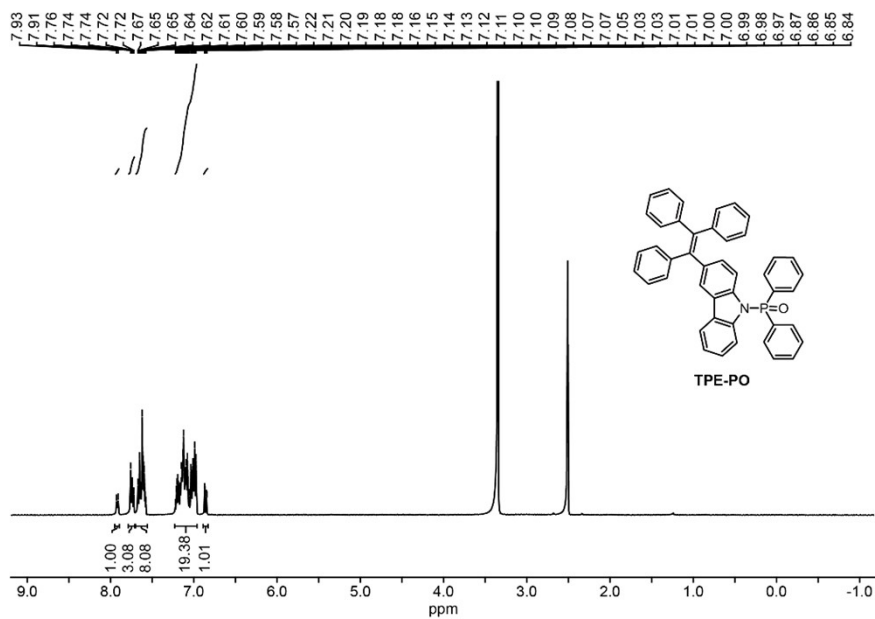**Figure S6**. ^{1}H NMR spectrum of **TPE-PO** in DMSO- d_6.
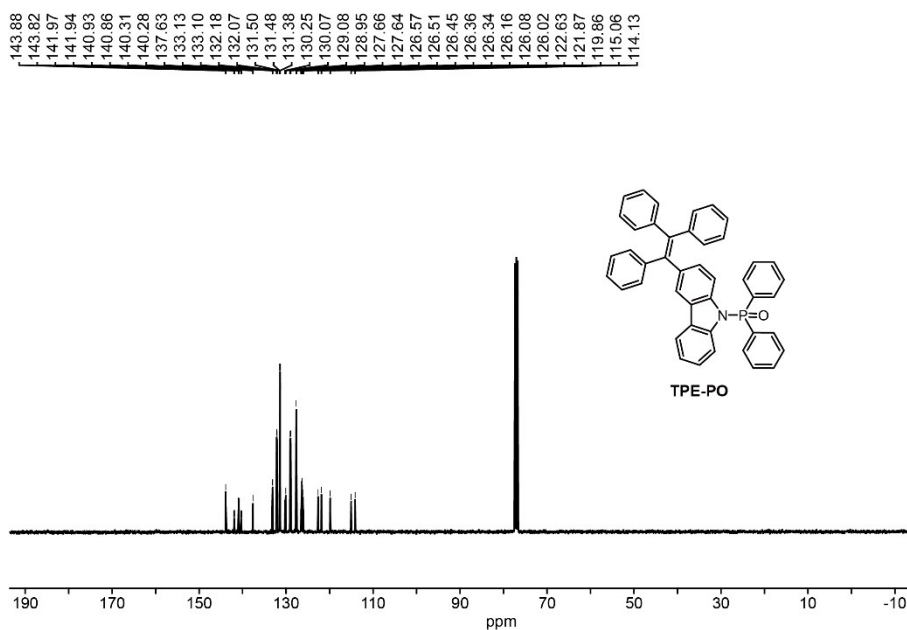

Figure S7. ^{13}C NMR spectrum of **TPE-PO** in CDCl$_3$.
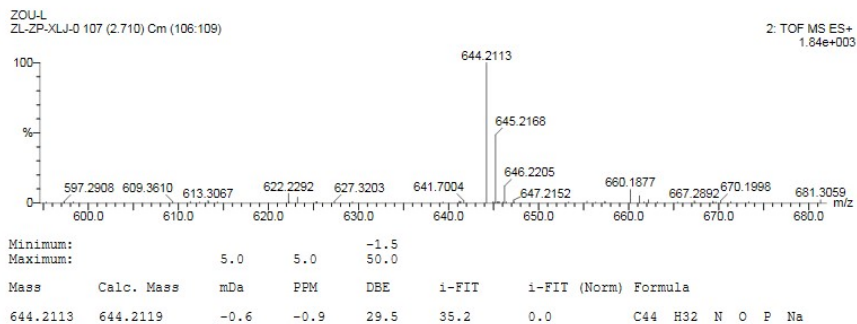

Figure S8. HRMS spectrum of **TPE-PO**.

Synthesis of diphenyl(3-(1,2,2-triphenylvinyl)-9*H*-carbazol-9-yl)phosphine sulfide (TPE-PS)

TPE-PS was prepared by sulfuring **TPE-P** (2.00 g, 3.30 mmol) using sulfur (0.16 g, 4.95 mmol) in an identical synthetic procedure in preparing **TPE-PO**, except that sulfur was adopted instead of H_2O_2.[5] Yield: (1.83 g, 87%). ^1H NMR (DMSO- d_6, 400 MHz) δ (ppm): 8.02 (m, 5H), 7.76 (m, 3H), 7.64 (m, 4H), 7.23 (m, 17H), 6.69 (d, J = 8 Hz, 1H), 6.55 (d, J = 8 Hz, 1H), 6.18 (d, J = 8 Hz, 1H). ^{13}C NMR (CDCl$_3$, 100 MHz) δ (ppm): 143.91, 143.79, 141.55, 141.52, 140.88, 140.73, 140.04, 137.40, 132.92, 132.68, 132.63, 132.51, 131.91, 131.49, 131.37, 131.33, 129.53, 129.07, 128.93, 127.70, 127.65, 126.96, 126.91, 126.43, 126.36, 125.63, 122.68, 121.78, 119.88, 115.47, 114.29. HRMS (EI): m/z calcd for C$_{44}$H$_{32}$NPS $[M]^+$: 637.1993; found: 637.1992.
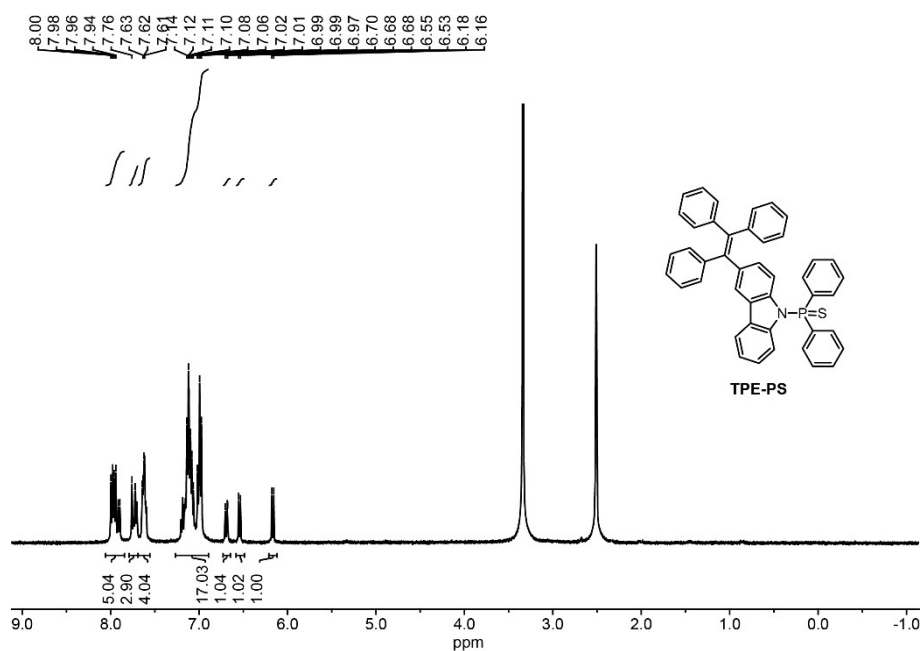

Figure S9. ^1H NMR spectrum of **TPE-PS** in DMSO- d_6.
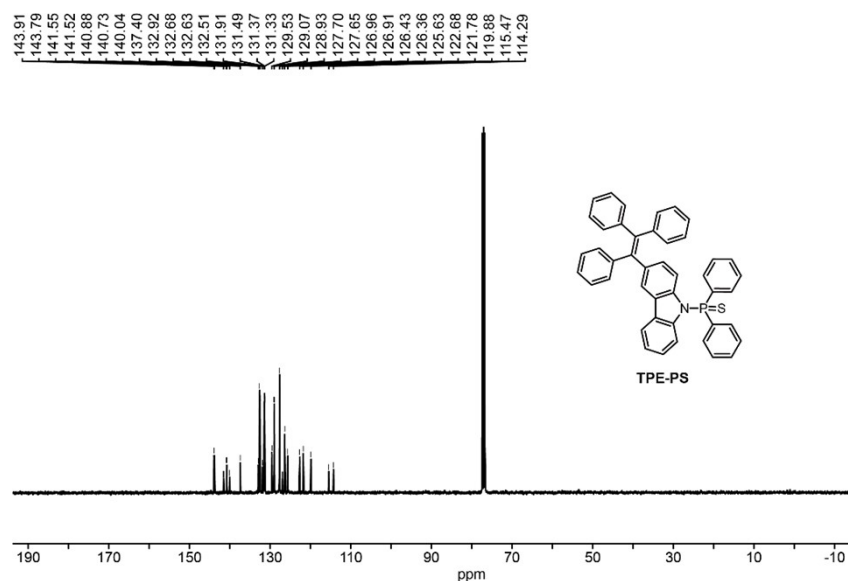
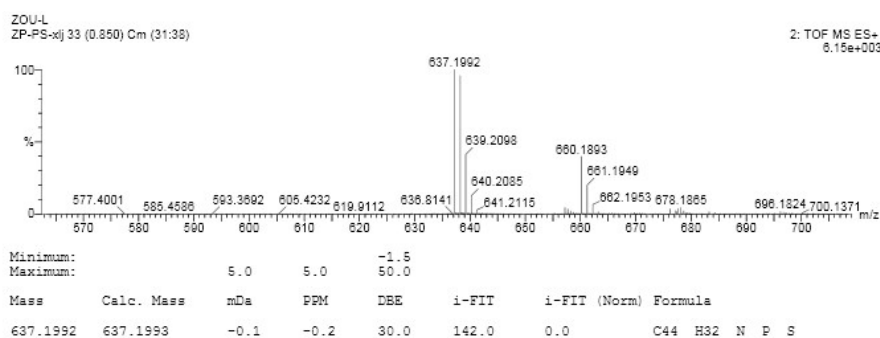**Figure S10.** ^{13}C NMR spectrum of **TPE-PS** in CDCl$_3$.

Figure S11. HRMS spectrum of **TPE-PS**.

2. Thermal stabilities

Thermal properties of the AIE-active resonance molecules were investigated by thermogravimetric analysis (TGA) and differential scanning calorimetry (DSC). TGA measurements were conducted on a DTG-60 Shimadzu thermal analyst system under a heating rate of 10°C /min and a nitrogen flow rate of 50 cm^3/min. DSC analyses were performed on a Shimadzu DSC-60A instrument under a heating rate of 10°C /min and a nitrogen flow rate of 20 cm^3/min. Temperature at 5% weight loss was used as the decomposition temperature (T_d). The glass transition temperature (T_g) was determined from the first heating scan. As shown in Figure S12, all materials show good thermal stability with T_ds of 324°C, 342°C and 344°C for **TPE-P**, **TPE-PO** and **TPE-PS**, respectively. Meanwhile, **TPE-P**, **TPE-PO** and **TPE-PS** show glass transition process with high T_gs of 211°C, 228°C and 220°C, respectively.
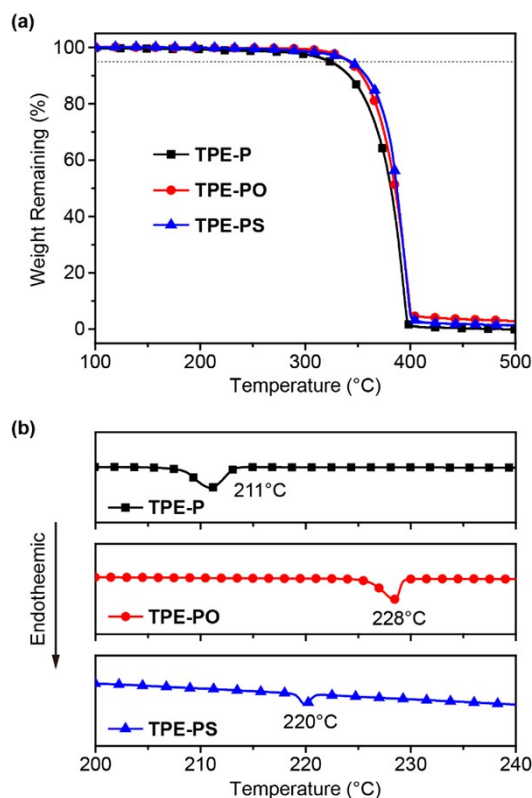
Figure S12. (a) TGA and (b) DSC curves of the AIE-active resonance molecules.

3. Photophysical properties

Ultraviolet-visible (UV-Vis) spectra were recorded on a JASCO V-750 spectrophotometer, while fluorescence spectra were obtained on an Edinburgh FLS980 fluorescence spectrophotometer with a Xenon lamp as light source. Transient PL decay curves were collected using an Edinburgh FLS 980 fluorescence spectrophotometer at room temperature under the excitation wavelength of 295 nm. The absolute photoluminescence quantum yield (PLQY) was obtained using an integrating sphere. The lifetimes of the luminescence were figured out by fitting the luminescent intensity decay curve (I(t)) with a multi-exponential decay function in Equation S1:

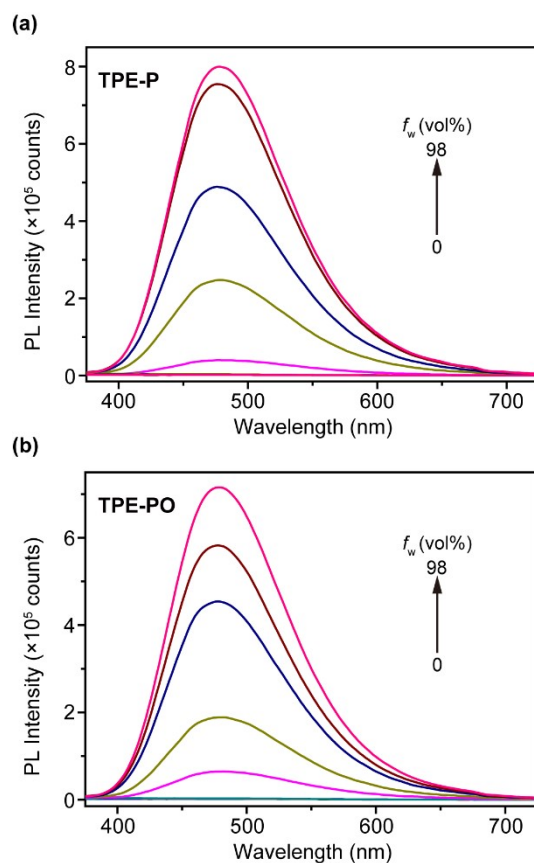$$I(t) = \sum_i A_i e^{-\frac{t}{\tau_i}} \qquad (S1)$$

Figure S13. Steady-state PL spectra of (a) **TPE-P** and (b) **TPE-PO** in THF/water mixtures with different volume fractions of water (f_w) under the excitation of 320 nm UV light.
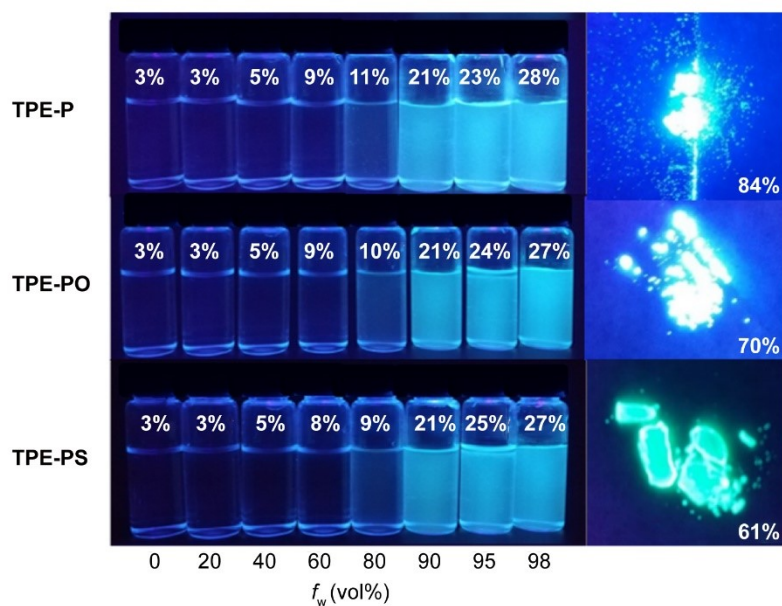

Figure S14. PLQYs of AIE-active resonance molecules in THF/water mixtures (left) and in crystals (right).

Table S1. Thermal and photophysical properties of the AIE-active resonance molecules.

Compound	T_d/T_g (°C)	λ_{abs} (nm)		$E_g{}^a$ (eV)	λ_{em} (nm)		PLQY (%)		
		CH_2Cl_2	Film		CH_2Cl_2	Film	THF	THF/water (2/98, v/v)	Crystal
TPE-P	211/323	300,320	302,327	3.23	394,413	483	3	28	84
TPE-PO	228/342	300,320	302,327	3.23	394,413	481	3	27	70
TPE-PS	220/344	300,320	302,327	3.23	403,418	477	3	27	61

[a]Optical bandgap (E_g) calculated by the absorption edge technique in CH_2Cl_2. (2/98, v/v).

4. Explosive detection properties

The explosive detection of PA was measured in a THF/water (95/5, v/v) mixture (10 μM) of the AIE-active resonance molecules by gradually adding PA (0-60 μM for **TPE-P**, 0-54 μM for **TPE-PO** and 0-48 μM for **TPE-PS**) at room temperature. The limit of detection (LOD) was determined by using equation: LOD = $3\delta/K$, where δ is the standard deviation of ten blank measurements, and K is the slope of the calibration curve.

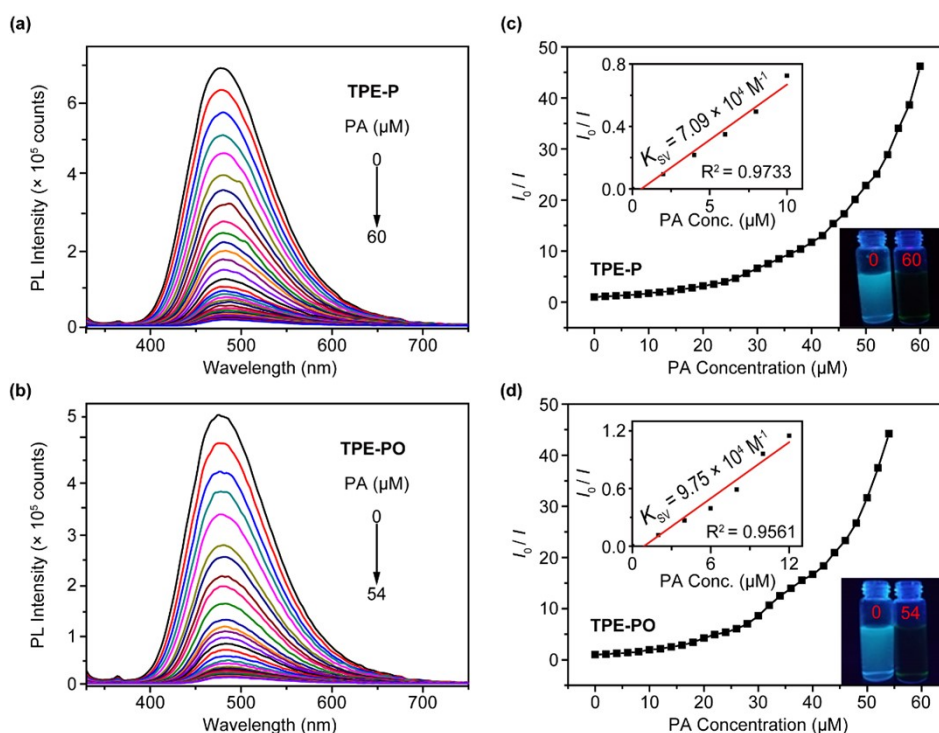**Figure S15**. PL spectra of (a) **TPE-P** and (b) **TPE-PO** (10 μM) excited at 320 nm with various concentrations of PA. Stern-Volmer plots of I_0/I for (c) **TPE-P** and (d) **TPE-PO** with PA (I_0 is the PL intensity without PA; I is the PL intensity at variable concentrations of PA). Insets: Stern-Volmer plots at lower concentration of PA in linear range and PL photographs with different PA concentrations in μM.
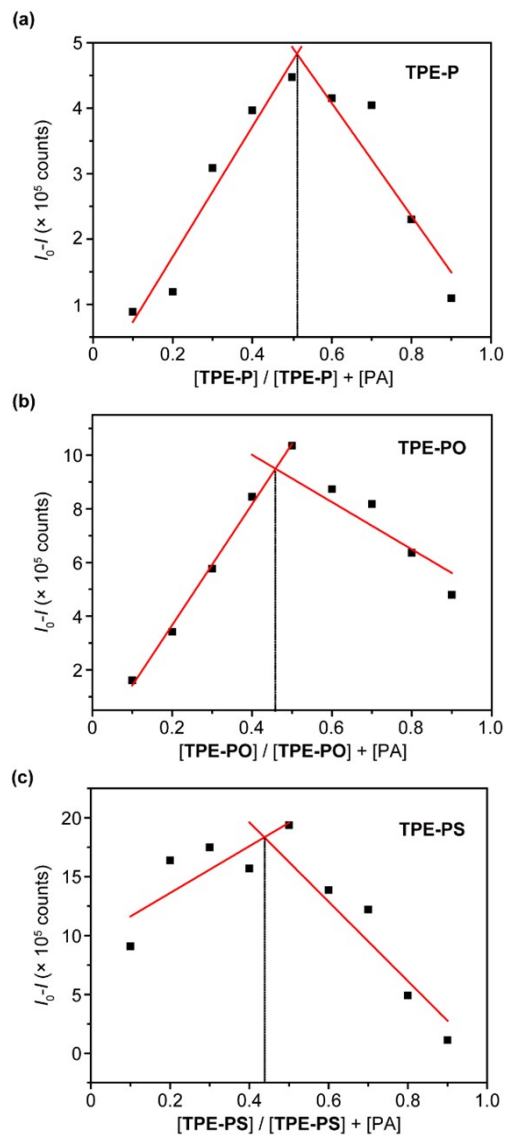
Figure S16. Job's plot obtained by recording the fluorescence intensity at 480 nm for the solution of (a) **TPE-P**, (b) **TPE-PO**, and (c) **TPE-PS** with PA in a binary solvent of THF/water (v/v, 5/95) at room temperature. [**TPE-P**, **TPE-PO** or **TPE-PS**] + [PA] = 1.0×10^{-5} M.
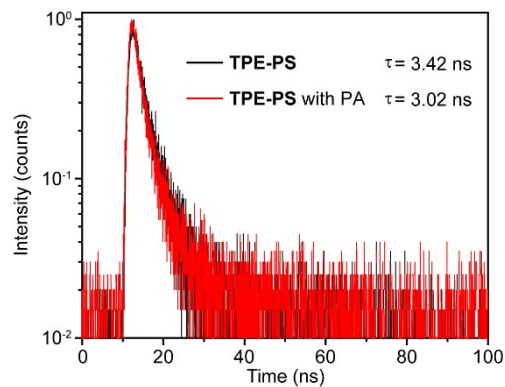

Figure S17. Transient PL decay curves of **TPE-PS** at 480 nm with (red) or without (black) PA. The excitation wavelength is at 320 nm.

Table S2. A brief summary of the reported detection performance of PA.

Fluorophores	Solvent	λ_{em} (nm)	K_{SV} (M^{-1})	LOD (nM)	References
PFTPBZ	Water/THF	500	7.6×10^3	474	[6]
3a	Water/THF	~638	7.0×10^4	310	[7]
3b	Water/THF	635	1.54×10^5	61	[7]
3c	Water/THF	~638	6.1×10^4	330	[7]
3d	Water/THF	~638	4.4×10^4	460	[7]
TBAFP1	THF	386	5.3×10^5	144	[8]
TBAFP2	THF	425	2.4×10^5	151	[8]
DBA	Water/THF	585	7.4×10^3	72	[9]
TL18	DMSO	530	-	63	[10]
TNQ	Water/DMF	460	7.4×10^4	47	[11]
TPE-P	Water/THF	477	7.09×10^4	70	**This work**
TPE-PO	Water/THF	478	9.75×10^4	55	**This work**
TPE-PS	Water/THF	478	1.33×10^5	31	**This work**

5. Dynamic detection mechanism

Cyclic voltammetry (CV) measurements were performed at room temperature on a CHI660E system in a typical three-electrode cell with a working electrode (glass carbon), a reference electrode (Ag/Ag$^+$, referenced against ferrocene/ferrocenium (FOC), and a counter electrode (Pt wire) in acetonitrile solution of tetrabutylammonium hexafluorophosphate (Bu$_4$NPF$_6$) (0.1 M) at a sweeping rate of 100 mV s^{-1}. HOMO energy levels (E_{HOMO}) of the materials were estimated based on the reference energy level of ferrocene (4.8 eV below the vacuum) according to Equation S2:

$$E_{HOMO} = - (E_{onset}^{Ox} - E_{(Fc/Fc^+)} + 4.8)\ eV \tag{S2}$$

where $E_{(Fc/Fc^+)}$ is the onset potential of oxidative wave of ferrocene (Fc) *vs* Ag/Ag$^+$ and E_{onset}^{Ox} is the onset potential of the oxidation wave of the materials deposited as thin films on the surface of the working electrode. LUMO energy level (E_{LUMO}) was estimated by adding the optical bandgap (E_g) to the corresponding HOMO energy level as in Equation S3:

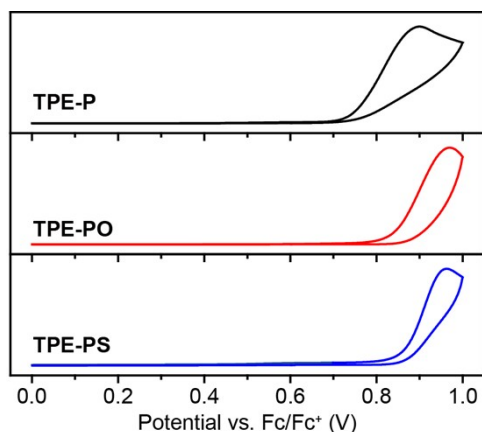$$E_{LUMO} = E_{HOMO} + E_g \tag{S3}$$

Figure S18. Cyclic voltammograms of the AIE-active resonance molecules.

DFT calculations

Density functional theoretical (DFT) calculations were performed on Gaussian 09 program. The highest occupied molecular orbital (HOMO), the lowest unoccupied molecular orbital (LUMO) energy levels, and frontier molecular orbital distributions were predicted by B3LYP/6-31G(d) based on the optimized ground state (S_0) geometries, since B3LYP/6-31G(d) is good in predicting the molecular energy levels of organic optoelectronic molecules.[12]
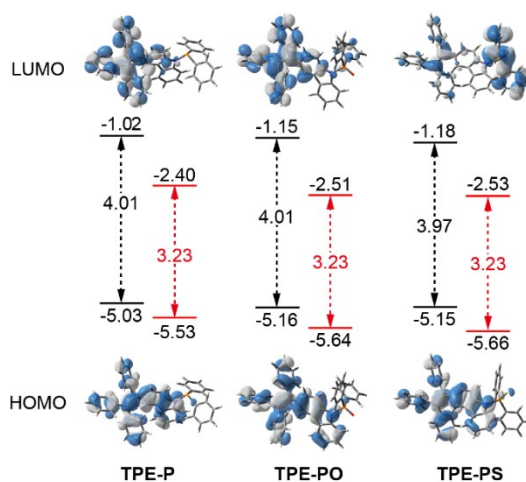

Figure S19. Theoretical (in black) and experimental (in red) HOMO and LUMO energy levels as well as the frontier molecular orbitals distributions of the AIE-active resonance molecules.

Fuzzy bond order analysis embedded in Multiwfn was used to study the bond order of the resonance structures based on the optimized molecular structures at the ground state (S_0). NBO 6.0 program was used to perform NBO energetic analysis with B3LYP/6-31G(d) method based on the optimized molecular structures at the ground state (S_0). The energy of the resonance variation (E_{RV})

was estimated using the energy difference of idealized natural Lewis structure of N-P=X and N$^+$-P=X$^-$ by deleting all Fock matrix elements between Lewis NBOs and the vicinal non-Lewis NBOs.[13]

Table S3. Fuzzy bond order analysis of the AIE-active resonance molecules.

Compound	Bond order		
	N-P	P=X[a)]	C-P
TPE-P	1.25	-	1.09/1.10
TPE-PO	1.21	2.15	1.042/1.043
TPE-PS	1.21	1.88	1.02/1.03

[a)] X is O in **TPE-PO**, and S in **TPE-PS**.

Table S4. Energy of the resonance variation (E_{RV}) between N-P=X and N$^+$-P=X$^-$ resonance structures (X=O or S).

Compound	Structure	Energy (a.u.)	E_{RV} (eV)
TPE-PO	N-P=O	-2151.14345329	2.20
	N$^+$=P-O$^-$	-2151.06251124	
TPE-PS	N-P=S	-2473.75834123	0.99
	N$^+$=P-S$^-$	-2473.72177764	

6. References

1   H. Liu, Y. Gu, Y. Dai, K. Wang, S. Zhang, G. Chen, B. Zou, B. Yang. *J. Am. Chem. Soc.* 2020, **142**, 1153.

2   C. Wu, W. Liu, K. Li, G. Cheng, J. Xiong, T. Teng, C.M. Che, C. Yang. *Angew. Chem. Int. Ed.* 2021, **60**, 3994.

3   Y. Tao, J. Xiao, C. Zheng, Z. Zhang, M. Yan, R. Chen, X. Zhou, H. Li, Z. An, Z. Wang, H. Xu, W. Huang. *Angew. Chem. Int. Ed.* 2013, **52**, 10491.

4   Y. Li, Z. Li, J. Zhang, C. Han, C. Duan, H. Xu. *Adv. Funct. Mater*. 2021, **31**, 2011169.

5   Y. Tao, L. Xu, Z. Zhang, R. Chen, H. Li, H. Xu, C. Zheng, W. Huang. *J. Am. Chem. Soc.* 2016, **138**, 9655-9662.

6   Y. Li, Y. Zhang, Y. Zhang, Z. Wang, H. Yang, H. Yao, T. Wei, Q. Lin. *Dyes Pigments* 2020, **181**, 108563.

7   S. Chen, K. Jiang, J. Lin, K. Yang, X. Cao, X. Luo, Z. Wang. *J. Mater. Chem. C* 2020, **8**, 8257-8267.

8   M. Ansari, R. Bera, S. Mondal, N. Das. *ACS Omega* 2019, **4**, 9383−9392.

9   M. Shyamal, D. Das, P. Giri, S. Maity, A. Misra. *Mater. Today Chem*. 2019, **14**, 100193.

10   A. Kathiravan, A. Gowri, T. Khamrang, M. Kumar, N. Dhenadhayalan, K. Lin, M. Velusamy, M. Jaccob. *Anal. Chem.* 2019, **91**, 13244−13250.

11   L. Adil, P. Gopikrishna, P. Iyer. *ACS Appl. Mater. Interfaces* 2018, **10**, 27260−27268.

12   G. W. T. M. J. Frisch, H. B. Schlegel, G. E. Scuseria, M. A. Robb, J. R. Cheeseman, G. Scalmani, V. Barone, G. A. Petersson, H. Nakatsuji, X. Li, M. Caricato, A. Marenich, J. Bloino, B. G. Janesko, R. Gomperts, B. Mennucci, H. P. Hratchian, J. V. Ortiz, A. F. Izmaylov, J. L. Sonnenberg, D. Williams-Young, F. Ding, F. Lipparini, F. Egidi, J. Goings, B. Peng, A. Petrone, T. Henderson, D. Ranasinghe, V. G. Zakrzewski, J. Gao, N. Rega, G. Zheng, W. Liang, M. Hada, M. Ehara, K. Toyota, R. Fukuda, J. Hasegawa, M. Ishida, T. Nakajima, Y. Honda, O. Kitao, H. Nakai, T. Vreven, K. Throssell, J. A. Montgomery, Jr., J. E. Peralta, F. Ogliaro, M. Bearpark, J. J. Heyd, E. Brothers, K. N. Kudin, V. N. Staroverov, T. Keith, R. Kobayashi, J. Normand, K. Raghavachari, A. Rendell, J. C. Burant, S. S. Iyengar, J. Tomasi, M. Cossi, J. M. Millam, M. Klene, C. Adamo, R. Cammi, J. W. Ochterski, R. L. Martin, K. Morokuma, O. Farkas, J. B. Foresman, and D. J. Fox. *Journal*, 2016, Revision D.01.

13   T. Lu, F. Chen, *J. Comput. Chem*. 2012, **33**, 580.